

High Rotation Speed Friction Stir Welding for 2014 Aluminum Alloy Thin Sheets

Shujin Chen, Yang Zhou, Junrong Xue, Ruiyang Ni, Yue Guo, and Jianghui Dong

(Submitted June 2, 2016; in revised form December 11, 2016; published online February 3, 2017)

In this study, 2014 aluminum alloy sheets with 1 mm thickness are welded successfully by friction stir welding (FSW) robot under the condition of high rotation speed. When the high rotation speed of 10,000–16,500 rpm is applied, the lower axial pressure (less than 200 N) is obtained, which reduces stiffness requirements for equipment. Welding deformation is inevitable because high rotation speed can easily result in rapid heating rate and uneven heat input. The welding distortion caused by two cooling methods is measured, respectively, by laser range finder. The experimental results show that the welding distortion is smaller under the condition of water cooling. When the rotation speed is up to 15,000 rpm and welding speed 50–170 mm/min, the whole welding process is controllable. Under the higher rotation speed condition, the welding defects disappear gradually and more stable mechanical properties can be obtained up to 75% of base metal ($\omega = 16,000$ rpm, $v = 110$ mm/min). The results of different welding parameters demonstrate that the high rotation speed can increase material mixing and reduce the axial force (z force), and it can benefit lightweight sheet welding by using FSW robot.

Keywords aluminum alloy, friction stir welding, high rotation speed, mechanical behavior, thin sheet

1. Introduction

As FSW evolved through two decades after its discovery, it has become a viable manufacturing technology for the structural assembly of metallic sheet and materials for applications in various industries, including aerospace, automobile and shipbuilding. As Rajakumar et al. (Ref 1) and Cam et al. (Ref 2, 3) suggested, FSW can achieve solid-state welding without filler materials, which effectively avoids cracks and porosity defects. Actually, the FSW machine is developed to be more efficient and automated. At the same time, the current state of the art of FSW is developing beyond Al alloys, including Mg alloys, Cu alloys, steels, Ti alloys and metal matrix composites, focusing particularly on microstructural aspects, joints properties, material flow and material selection for tooling. The basic principle of FSW is associated with plunging a rotating tool into the workpiece. The rotating tool pin slowly penetrates the workpiece until the tool shoulder touches the top surface of the workpiece; then, it is held there while the metal around is being softened by generated frictional heat. Subsequently, the tool traverses along the weld seam and the weld is formed under the heat and plastic deformation. Since FSW uses a rotating tool, similarly to how a milling machine uses an end mill, computer

numerically controlled milling machines could immediately be used for the welding process and a lot of valuable efforts were placed on how best to automate the process for further adoption. FSW robots have advantages of low cost, good dexterity and flexibility and play a very important role in advanced automatic welding process.

Traditional FSW typically involves rather large process forces, and thus, the welding process was limited to rather large milling machines. Su et al. (Ref 4) recognized that the z force of the conventional friction stir welding goes up to 7000 N, which will inevitably lead to thinning phenomenon and serious flash. In addition, Zhang et al. (Ref 5) pointed out traditional FSW process requires larger plunge depth compared with those of the high rotation speed FSW, so thickness problem is inevitable in the FSW process of thin sheets. Ramulu et al. (Ref 6) measured the z force during FSW process of 2-mm aluminum alloy sheets, and the z force still remained 4000 N. Guillo et al. (Ref 7) conducted the FSW process of 3-mm aluminum alloy sheets on the robot system, and the z force reached 3000 N. Obviously, the relatively high force requirements of FSW still pose particular challenges for implementation of FSW robots. In general, the stiffness of the robot arm is insufficient. So reducing the z force can be beneficial to the FSW operation. Thin sheet is more likely to be welded successfully while plunge depth may reduce the strength of the joint. So it is significant to reduce the z force and the plunge depth especially for the thin sheet welding.

As suggested in the previous research, the high rotation speed can also reduce the z force. According to Wang et al. (Ref 8) and Cao et al. (Ref 9), the rotation speed can greatly affect the welding process and joint quality, and the amount of the z force decreases with the increase in rotation speed in the stable welding process. He et al. (2011) carried out FSW high rotation speed welding tests on LF21 aluminum alloy sheets with thickness of 1.5 mm. It was the first time to put forward a welding process with rotation speed of 5000 r/min (Ref 10). Zhao et al. (Ref 11) argued that high rotation speed FSW had advantages of fast heating rate, less welding joints defects, good mechanical properties and so on. According to the

Shujin Chen, Yang Zhou, Junrong Xue, and Ruiyang Ni, School of Material Science and Engineering, Jiangsu University of Science and Technology, Zhenjiang 212003, China; Yue Guo, Hua Heng Welding Technology Co. Ltd, Kunshan 215300 Jiangsu Province, China; and Jianghui Dong, School of Natural and Built Environments, University of South Australia, Adelaide, SA 5095, Australia. Contact e-mails: chenshujin7120@126.com and jianghui.dong@mymail.unisa.edu.au.

research of Qin et al. (Ref 12), under the condition of the same amount of heat input, joints with higher strength were obtained at higher rotation speed.

However, the high rotation speed FSW is different to conventional FSW. As stated by Yan et al. (Ref 13), due to uneven heat input, welding distortion of the thin sheets may occur during the high rotation speed FSW process. In order to

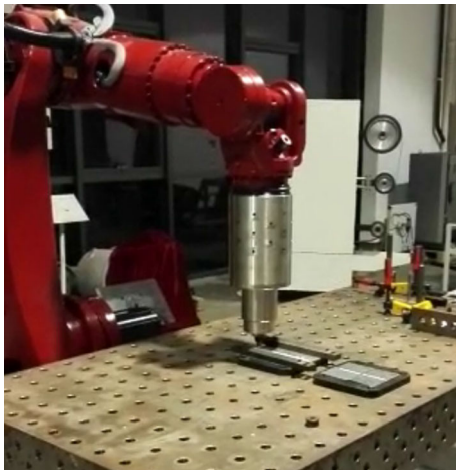


Fig. 1 Robotic FSW system

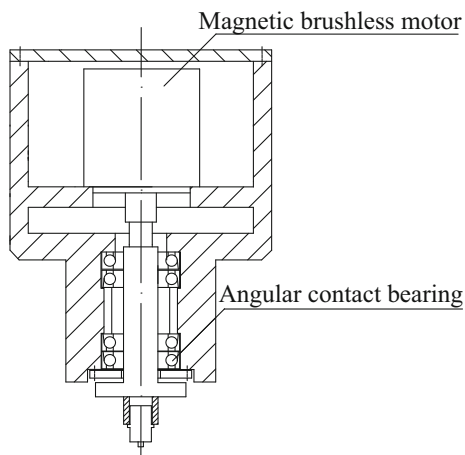
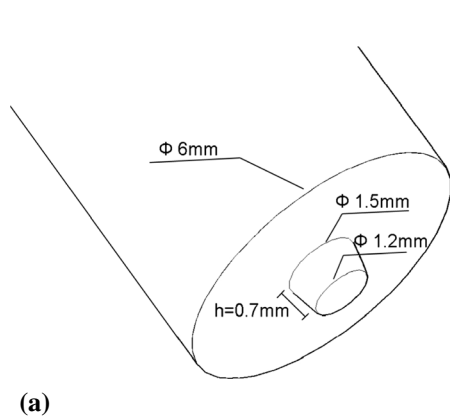
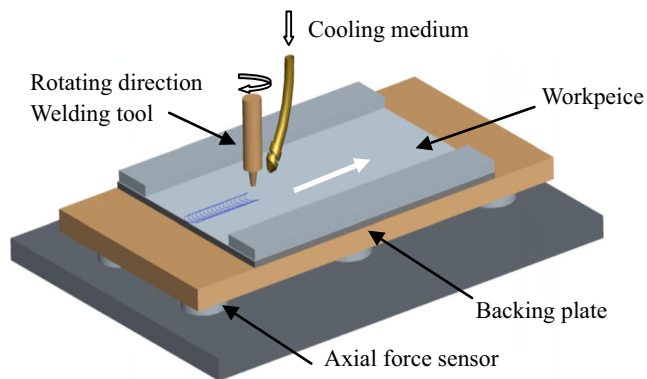


Fig. 2 Welding tool



(a)



(b)

Fig. 3 Schematic of FSW tool and FSW process (a) FSW tool, (b) FSW process

control distortion, Zhang et al. (Ref 14) tested the welding quality of submerged and found that the location of HAZ was moved toward the weld center. He et al. (Ref 15) also carried out FSW of 2024-T4 aluminum alloy with 1.8 mm thickness, showing that water cooling device can effectively control the local welding temperature field, the peak value of residual stress and residual stress in welding constraints zone and ultimately reduce the macrodeformation of weld. Chen et al. (Ref 16) implemented temperature measurement and control of bobbin tool friction stir welding by changing rotation speed, but the influence of the larger shoulder on the welding quality was not the same as the thin sheet. Therefore, it is particularly significant to choose the suitable welding method for thin aluminum alloy sheets.

On the basis of the literature review above, the high rotation speed FSW is an effective way to achieve satisfactory joint of sheets, but a large z force may hinder its application in the robot. It will further expand and enrich FSW technology and is also helpful to realize lightweight welding by extending the range of welding parameters, improving the cooling method and revealing the characteristics of the z force of the welding process.

This study is to investigate higher rotation speed FSW (10 times or more than 10 times as much as the rotation speed of the conventional FSW) of 2014 aluminum alloy sheet, to explore the characteristics of z force during the welding process and verify the feasibility of the robot welding in FSW with low z force. Since 2014 aluminum alloy sheet is of high strength and high heat intensity, it has been widely used in the fields of aviation, energy and transportation. As mentioned by Zhao et al. (Ref 17), it was now widely used for aeronautic and aerospace engineering, for example, rocket fuel tank and aircraft envelope. As such, this paper intends to investigate the feasibility of the high rotation speed FSW process with different cooling methods and illuminate the process characteristics from the perspectives of microstructure evolution and mechanical behavior of FSW joints. Smaller welding distortion and lower z force are obtained, and the intrinsic reasons for the process characteristics are also clarified.

2. Experiment

A payload capacity robot (Kunshan-1-150 kg) was chosen in this study, and the photograph of this robotic FSW system is

shown in Fig. 1. This robot has open architecture (high level programming language), which would allow for routines to be written to overcome unknown reactions during the FSW process. In order to make full use of the entire system's mechanical stiffness, the distance from the wrist to the FSW tool is 530 mm. Due to the unknown capability of the robot to perform FSW, the rotary power source was crucial. To meet this constraint, a magnetic brushless motor (5000 W) driven by square wave current with 0 to 18,000 rpm range was chosen. The spindle of the motor transferred the driving force to FSW tool. As the most important end effector in robot system, the welding tool should have sufficient capacity to bear z force, so four matched angular contact bearings can be adopted to provide good radial and thrust capabilities (Fig. 2).

Previous studies have suggested that the best quality weld was acquired using the taper pin with screw thread, as the appearance of the weld was good, and no obvious defects were found (Ref 18). In addition, the small tool size is especially suitable for the thin sheets welding according to the studies of the influences of pin shapes and tool geometry on properties of joint (Ref 19-21). The screw thread is too difficult to make on the mini-sized pin. Thus, a FSW tool with a 6-mm-diameter shoulder and conical pin with 0.7-mm-length pin was chosen. Detailed characteristics of the shoulders are schematically illustrated in Fig. 3. The cooling device includes an air compressor, a cooling water pipe and an atomizing nozzle. When the cooling water pipe is closed, it produces high pressure gas. When the cooling water pipe is opened, it produces high pressure water mist.

The specimens used in this work were commercial 2014-T6 aluminum alloy sheets with thickness of 1 mm. Their nominal compositions (wt.%) are shown in Table 1. The main welding set is presented in Table 2.

The sheets with dimension of 100 mm × 80 mm were butt-welded under two different conditions: normal air cooling and water cooling. Three important parameters of friction stir

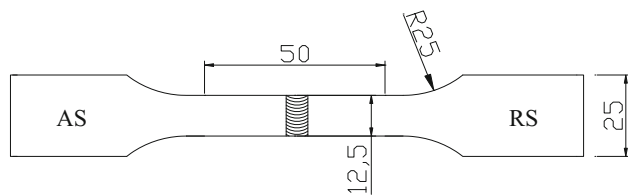


Fig. 4 Configuration and size of tensile specimen

welding such as rotation speed (ω), welding speed (v) and plunge depth (p) were considered in this study. The range of ω is 10,000-16,500 rpm, and p is maintained at 0.05 mm. During the whole welding process, v varies between 50 and 170 mm/min.

After welding, the longitudinal displacement and transversal displacement of the welding specimens were measured, respectively, by laser range finder with accuracy of 30 μ m. The principle of the laser range finder is shown in Fig. 5. Then, the cross sections of the joints were used for metallographic analysis and mechanical tests. The sample was cut from the joint center to both sides with width of 20 mm, which contains base metal (BM), heat affected zone (HAZ), thermal mechanical affected zone (TMAZ) and nugget zone (NZ). In order to evaluate the inner features of weld formation, the cross sections were polished using diamond pastes and etched with Keller's reagent (1 ml HF, 1.5 ml HCl acid 2.5 ml HNO₃ and 95 ml H₂O). The specimens were observed by a laser scanning confocal microscope and hyperfocal microscope. Microhardness profiles were measured on the polished cross sections by an automatic microhardness tester. Three transverse tensile specimens were prepared. The room temperature tensile test was carried out at a crosshead speed of 0.2 mm/min using an electron universal testing machine. The ultimate strength of joints was calculated based on the original sheet thickness but not the reduced section in the weld region. The size of the tensile specimen is shown in Fig. 4. In addition, the fracture of 2014 aluminum alloy thin-walled parts was analyzed by scanning electron microscope (SEM) analysis.

3. Results

3.1 Surface Appearance

A series of experiments were conducted when rotation speed is in the range of 10,000 to 13,500 rpm and welding speed is in the range of 50-90 mm/min. In these experiments, it is very

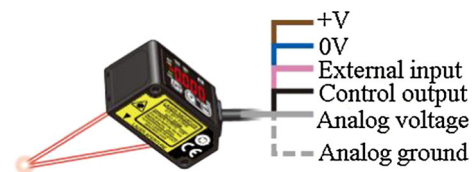


Fig. 5 Laser range finder

Table 1 Chemical composition of 2014 aluminum alloy (wt.%)

Cu	Si	Fe	Mn	Mg	Zn	Cr	Ti	Al	σ_b
4.5	0.50	0.50	0.8	1.4	0.25	0.10	0.15	Bal.	329 MPa

Table 2 Main welding set

Payload capacity of robot	Shape of welding tool	Drive motor of tool	Cooling air flow	Back plate	Axial force sensors
150 kg	Flat shoulder and tapered pin	A 5000-w brushless motor	35 L/min	Stainless steel	Six pressure sensors, each with 0-80 kg measuring range

difficult to control the welding process of aluminum alloy thin sheets. The results show that the weld formation of water cooling condition is better than that of air cool condition. However, no matter what the cooling conditions are, the groove defects will appear when ω is too small. Under the condition of water cooling, the groove defect appeared as shown in Fig. 6(a). The experimental results also suggest that flash tends to appear due to inappropriate parameters such as excessive plunge depth, as shown in Fig. 6(b) and (c). If the flash is very serious, the welding process has to be stopped. A good weld without distortion is shown in Fig. 6(d).

Meanwhile, surface warp is inevitable in the most welding process with air cooling condition (Fig. 7a). But different from fusion welding method, water cooling method can be used to control heating input of FSW process. When water cooling method is adopted, the distortion of the sheets is controlled basically (Fig. 7b).

The comparison test was carried out in the rotation speed of 15,000 and 16,000 rpm and welding speed of 100 mm/min, and the water flow rate is 3.2 ml/s. Figure 8 shows the distortion in the longitudinal and transversal directions under different cooling conditions. When the air cooling is used, the longitudinal deflection is 2 mm and the lateral deflection is 2.75 mm in the 16,000 rpm. When the water cooling is used, the minimum longitudinal deflection is 0.36 mm and the lowest transverse

deflection is 0.2 mm in the 15,000 rpm. In brief, the distortion of the air cooling is relatively larger than water cooling at the same rotation speed. Under the same cooling condition, the higher the rotation speed is, the higher distortion is.

From the above-mentioned experiment results, it can be concluded that it is difficult to obtain excellent welding joints under air cooling condition, such as serious warping and flash. Therefore, this study focuses on the mechanical properties, macrostructures and microstructure of welded joints under water cooling condition.

3.2 Tensile Properties

The tensile strength of the FSW 2014Al-T6 joints is shown in Fig. 9(a). As the figure shows, when ω is 15,000 rpm, the sample P1 has the peak tensile strength (σ_{P1}) of 211 MPa, and the corresponding welding speed (v_{P1}) is 100 mm/min. Similarly, σ_{P2} reaches 242 MPa when ω_{P2} is 16,000 rpm and v_{P2} is 110 mm/min, and σ_{P3} is 225 MPa when ω_{P3} is 16,500 rpm and v_{P3} is 130 mm/min. Figure 9 reveals three important findings. Firstly, for the FSW joints under the constant rotational rate, the tensile strength of the FSW joint reaches the peak value and then decreases with the increase in welding speed. Secondly, the welding speed, which corresponds to the peak tensile strength, increases with increasing rotation speed. Lastly, with

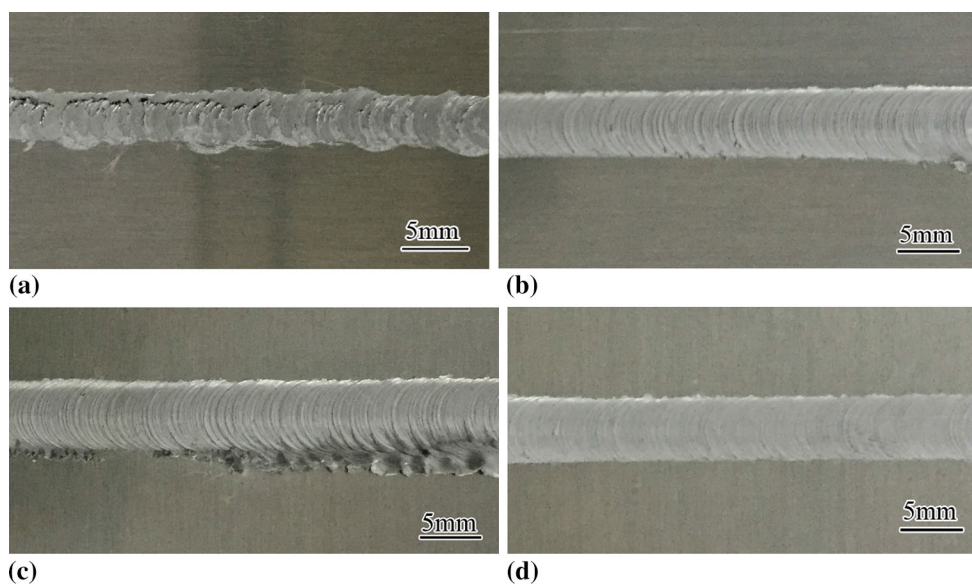


Fig. 6 Surficial morphologies of FSW 2014Al-T6 joints under water cool condition, (a) groove defects, (b) burr surface, (c) serious flash, (d) sound appearance

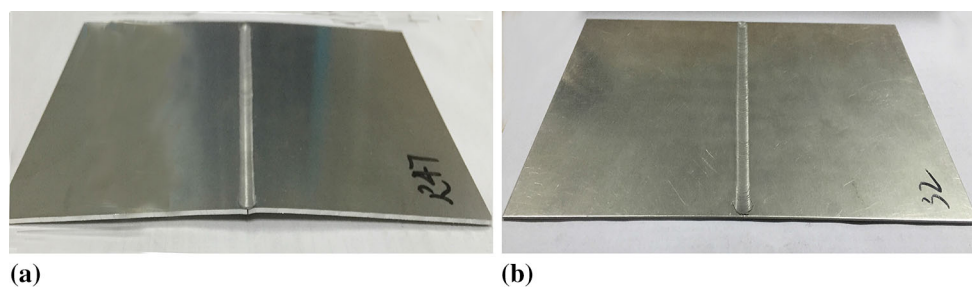


Fig. 7 Comparison of welding distortion (a) large distortion, (b) small distortion

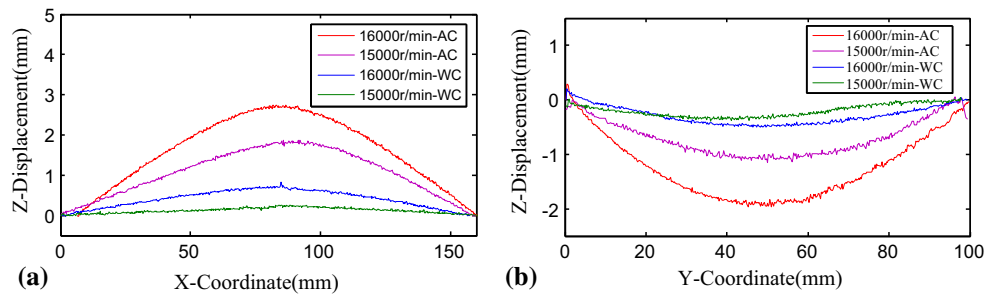


Fig. 8 Comparison of welding distortion (a) perpendicular to welding, (b) welding direction

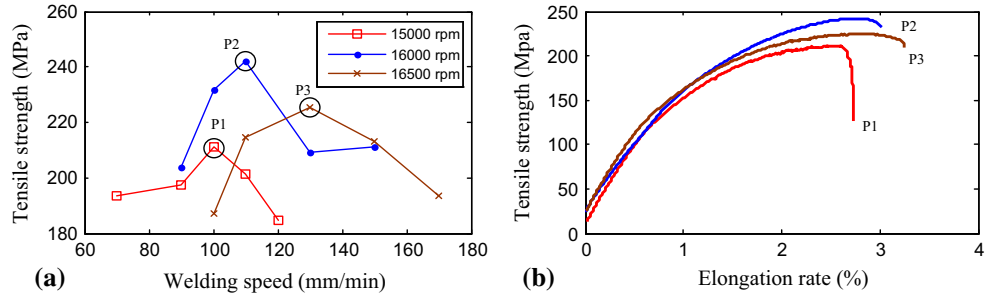


Fig. 9 Tensile properties of the welds (a) tensile strength trend, (b) tensile curves

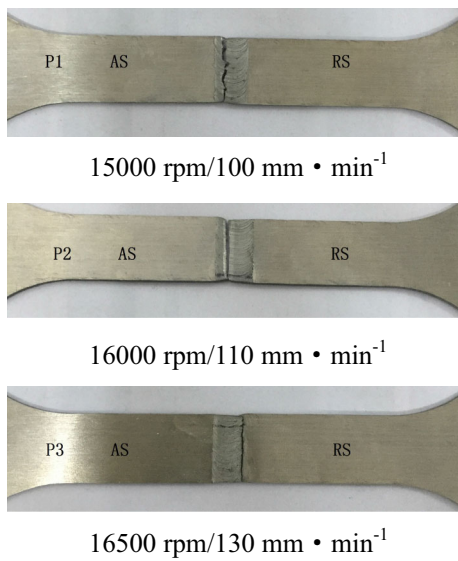


Fig. 10 Fracture specimen

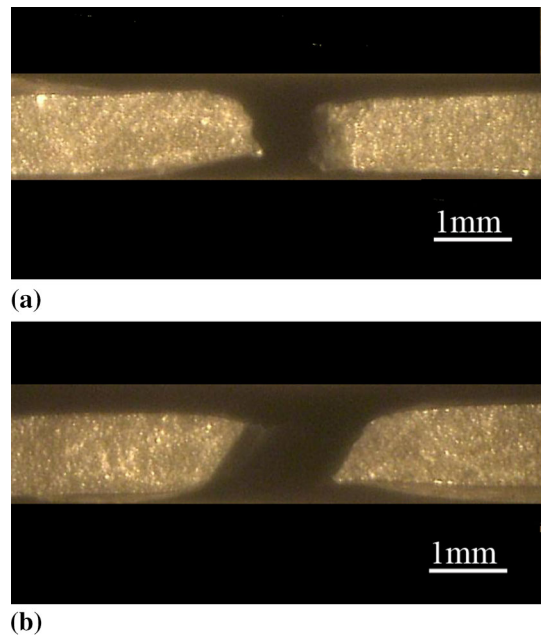


Fig. 11 Fracture macrograph (a) jagged tear fracture, (b) shear fracture

the increase in rotation speed, the peak value of tensile strength first increases and then decreases. Figure 9(b) shows that the elongation increases with the increases in rotation speed.

Different from the samples P1 and P2, the sample P3 fractured at the retreating side (RS), as shown in Fig. 10. The fracture mode of the specimens was divided into two: the first is jagged tear and the second shear fracture. The cross section of fracture samples is shown in Fig. 11.

3.3 Microstructure

Figure 12 shows the microstructure of the sample P2. Due to the high rotation speed of tool, the material mixing behavior

greatly enhanced during the welding process, and the grain size of the weld was not the same as the base metal.

As shown in Fig. 12(a), the grain size of the base material is elongated along the rolling direction. But the grain of NZ is smaller and uniform due to the strong material mixing effect of the tool (Fig. 12b), while the region between HAZ and TMAZ is not obvious. On the edge of NZ, the material had undergone plastic distortion, and then, the grains had been distorted and elongated, especially in the retreating side (Fig. 12c, d).

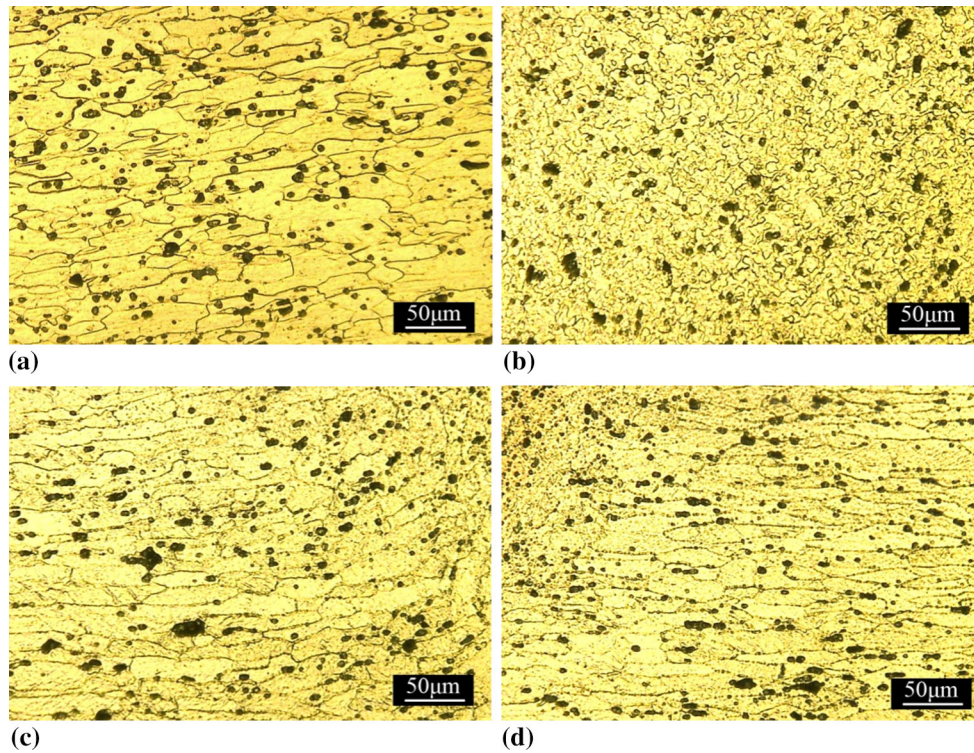


Fig. 12 Digital microscope microstructure of sample P2 (a) base metal, (b) nugget zone, (c) advancing side, (d) retreating side

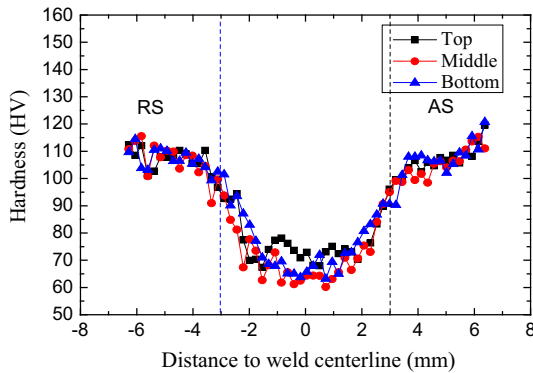


Fig. 13 Hardness distribution in the cross section of P2

3.4 Microhardness Map

Figure 13 shows the section hardness distribution of sample P2. The upper, middle and lower layers are at the distance to top surface of weld with 0.3, 0.5 and 0.7 mm, respectively, and the hardness testing load was 100 g for 15 s. The lowest hardness exists in the middle layer. For the middle layer, the average hardness of the NZ is 68 HV, lower than that of the conventional friction stir welding measured by Zhang et al. (Ref 14).

Compared with the hardness of the traditional friction stir welding joint, the “W” shape is not obvious. The lowest value is located in the nugget zone since the water cooling welding can reduce the solubility degree and promote the occurrence of subsequent aging.

4. Discussion

The internal defects such as root defects can be attributed to insufficient material flow around the tool. Material flow, not only depends on the ability of the tool to guide the deformed material toward the root of the weld, but also the degree of plasticization of the material. In turn, the heat is generated by the interface friction and plastic deformation of the material under the shoulder and depends on the welding parameters, in particular, the rotation speed and z force.

In this investigation, the weld defects appeared at rotation speed lower than 15,000 rpm, as shown in Fig. 14(a), because insufficient heat cannot provide good plasticization and proper flow of material. It is empirically clear that the higher rotation speed can produce more friction heat and the increase in heat input is able to avoid root defects.

However, when the rotation speed is 15,000 rpm, the internal defects still appear, as shown in Fig. 14(b), which directly leads to a low tensile strength. When the rotation speed is up to 16,000 rpm, the internal defects disappeared and the tensile strength was improved.

In this study, when the flat tool shoulder with 6 mm diameter was used, the change of z force in welding process was obtained, which is helpful to understand the characters of high rotation speed friction stir welding. The general law of the z force in different stages is similar to that of the conventional FSW, but the value is very low. As shown in Fig. 13, when the rotation speed is 15,000 rpm, the maximum value of the z force is only about 190 N. The z force increases during the tool plunge stage, reduces in preheating stage and subsequently increases to a stable value through water cooler at the normal welding stage. Like the findings of Wang et al. (Ref 8), with the

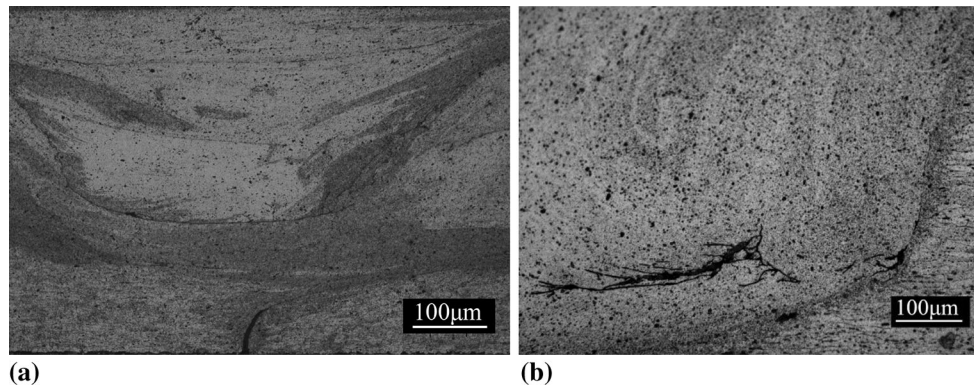


Fig. 14 Cross-sectional macrostructures of FSW 2014Al-T6 joints (a) root defect ($\omega < 15,000$ rpm), (b) internal defect ($\omega = 15,000$ rpm)

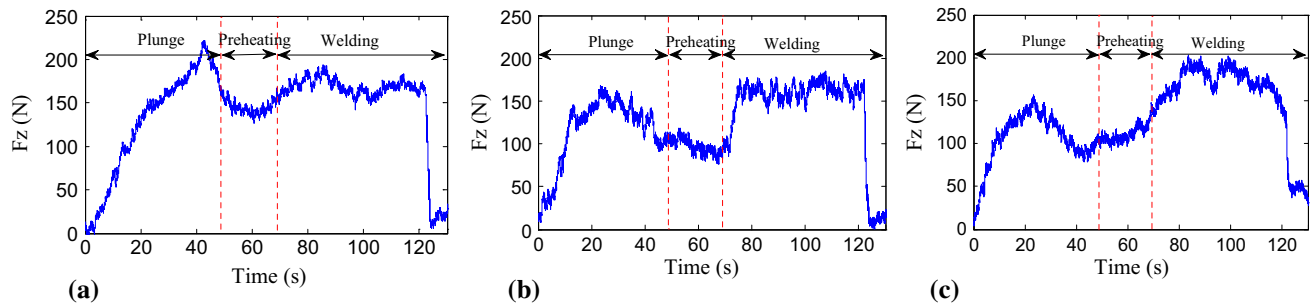


Fig. 15 Characteristic of axial force of friction stir welding with high rotation speed (a) rotation speed 15,000 rpm, (b) rotation speed 16,000 rpm, (c) rotation speed 16,500 rpm

increase in rotation speed, the z force presents an increasing trend in the stable welding process, and the effect of welding speed on z force is very small.

Figure 15(a), (b) and (c) shows z force corresponding to rotation speed 15,000, 16,000 and 16,500 rpm, respectively, when the welding speed is 110 mm/min. In the plunge and preheating stage, the higher rotation speed caused the lower z force. Under such a small z force, it is helpful to the operation of FSW robot with low stiffness. Due to weaker heat production in the lower rotation speed, internal defect still tends to appear when the rotation speed is 15,000 rpm although the z force of welding stage reached 190 N, as shown in Fig. 15(a). During the welding process, the rotation speed and water cooling affect the change of z force comprehensively. As the water cooling involved in welding stage, the z force rose quickly. Larger z force leads to better extrusion effect based on the precondition of adequate material flow, that is, a satisfactory joint can be obtained through sufficient heat production and appropriate z force, as shown in Fig. 15(b). However, more obvious mechanical vibration leads to the unstable z force when the rotation speed is 16,500 rpm, as shown in Fig. 15(c). Therefore, for the FSW robot, the stability of z force is also the guarantee of uniform joints as it can generate appropriate heat and better extrusion.

In conventional friction stir welding, the tensile strength of high strength aluminum alloy can reach 80%, but there are few reports about the thickness of 1 mm or less. The dynamic recovery and recrystallization occur in the nugget zone due to high temperature and stress, and the formation of grains is fine, so that the composite mechanical properties are improved. In

the heat affected zone, the precipitation phase has grown up under high thermal cycle and become the weakest area (Ref 22-24). For high rotation speed friction stir welding, grain refinement has also occurred in the nugget zone. In the heat affected zone, the grains only deform without obvious growth due to lower thermal cycles. However, the junction of heat affected zone and base metal is still the weakest region.

The fracture mode of the sample P1 is jagged tear (Fig. 16a), and the fracture mode of P2 and P3 is shear fracture (Fig. 16b). The jagged tear fracture is mostly seen in the advancing side attributed to the internal defect in NZ. However, shear fracture occurs on both sides of AS and RS. This fracture is due to the existence of low hardness zone (LNZ) (Ref 25). The shear fracture more inclines to occur on RS when the speed increases due to the more obvious deformation state grains in TMAZ. As shown in Fig. 16(c), the shallow dimples at the bottom of the jagged tear fracture caused reduction in integral joint strength. As shown in Fig. 16(d), at the middle of the jagged tear fracture is normal stress fracture, and the fracture mechanism of material is aggregation. And there are visible round dimples in microstructure, with the small dimples of different shapes around the big ones. The shear fracture has the characteristics of uniform dimples and elongated tear edge, which proved the good performance of joint as shown in Fig. 16(e).

As shown in the temperature curve in Fig. 17, under the condition of water cooling, the cooling effect is stronger than that of air cooling. In Fig. 17, the measure point was 5 mm away from the weld center. Therefore, it can be deduced that the high temperature range of nugget zone is different, the

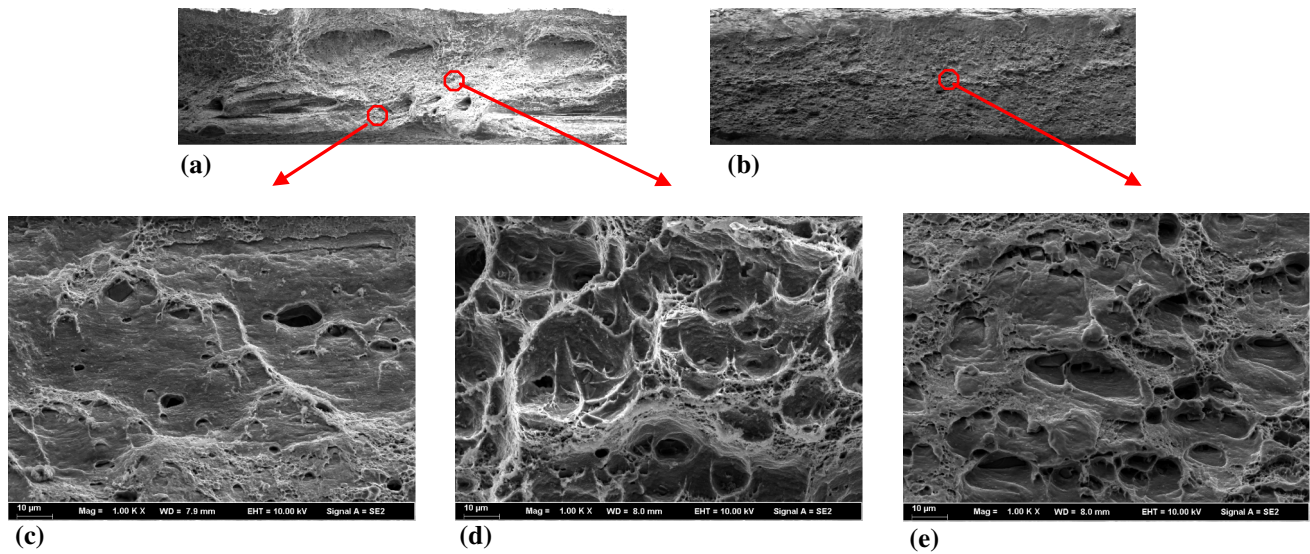


Fig. 16 SEM microstructure of tensile fracture (a) jagged tear fractorgraph, (b) shear fractorgraph, (c) morphology of bottom, (d) morphology of middle, (e) morphology of shear fracture

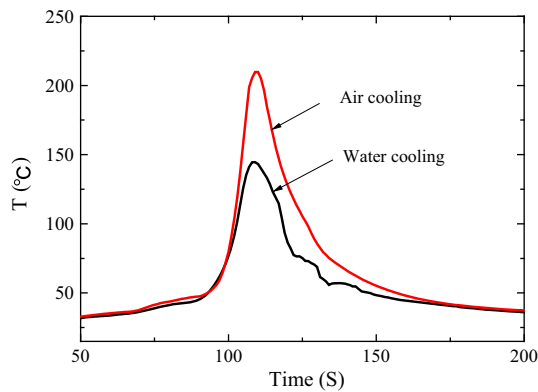


Fig. 17 Temperature curve of air and water cooling

wider is in air cooling, and the narrower is in water cooling. For heat treatment of high strength aluminum alloy, the original precipitates were partially dissolved, but the solid solubility and time effect of water-cooled weld nugget zone are weaker than those of air-cooled weld nugget zone. Different dissolubility of precipitates makes the lower hardness in water-cooled nugget, as explained by Song et al. (Ref 26).

In conclusion, only a small amount of plunge depth is needed to complete the welding under the condition of high rotation speed; besides, the thinning phenomenon is avoided and the z force is reduced greatly. The small z force is beneficial to the stability of the welding process and the reduction in the equipment rigidity. High rotation speed has another advantage of enhancing the material mixing. Therefore, a very small tool is competent to the task of welding. However, the results are not the same as expected. High rotation speed can also cause changes of the mechanical vibration. Besides, welding efficiency needs to be improved. The present work only puts forward the limited explanations on the important of the z force and water cooling method during thin sheets FSW. To conduct more thorough and accurate study will be an interesting topic in the future.

5. Conclusions

When the high rotation speed of 10,000-16,500 rpm is applied, the z force of welding stage is measured below 200 N. It is conducive to the FSW robot so as to achieve the lightweight thin sheet welding. Like the traditional FSW, the z force increases in the plunging process at first and decreases in the preheating process. The higher the rotation speed is, the smaller its peak is. In addition, the stability of z force is the guarantee of longitudinal uniform of joints and water cooling plays a significant role as it can reduce the accumulation of heat to prevent the decreasing of z force.

When 1-mm-thick 2014 aluminum alloy sheets are welded under high rotation speed with range of 10,000 to 16,500 rpm, only a small amount of plunge depth is needed to complete the welding. Thus, the thinning phenomenon is avoided and the z force is reduced greatly. Appropriate joint can be obtained easily by water cooling under the rotation speed of 16,000 rpm and welding speed of 110 mm/min. The grain deformation at the retreating side is significantly more than that at the advancing side.

Acknowledgments

This research was sponsored by Qing Lan Project and the National Natural Science Foundation of China (51675248, 51375218 and 51405206) and the Natural Science Fund of the Jiangsu Higher Education Institutions of China (15KJB460009).

Conflict of interests

The authors declare that they have no conflict of interests to this work.

References

1. S. Rajakumar, C. Muralidharan, and V. Balasubramanian, Establishing Empirical Relationships to Predict Grain Size and Tensile Strength of

- Friction Stir Welded AA 6061-T6 Aluminium Alloy Joints, *Trans. Nonferrous Met. Soc. China*, 2010, **20**, p 1863–1872
2. G. Çam and S. Mistikoglu, Recent Developments in Friction Stir Welding of Al-Alloys, *J. Mater. Eng. Perform.*, 2014, **23**, p 1936–1953
 3. G. Çam, Friction Stir Welded Structural Materials: Beyond Al-Alloys, *Int. Mater. Rev.*, 2011, **56**(1), p 1–48
 4. H. Su, C.S. Wu, A. Pittner, and M. Rethmeier, Simultaneous Measurement of Tool Torque, Traverse Force and Axial Force in Friction Stir Welding, *J. Manuf. Proc.*, 2013, **15**, p 495–500
 5. H. Zhang, M. Wang, W. Zhou, X. Zhang, Z. Zhu, T. Yu et al., Microstructure–Property Characteristics of a Novel Non-weld-Thinning Friction Stir Welding Process of Aluminum Alloys, *Mater. Des.*, 2015, **86**, p 379–387
 6. P.J. Ramulu, R.G. Narayanan, S.V. Kailas, and J. Reddy, Internal Defect and Process Parameter Analysis During Friction Stir Welding of Al 6061 Sheets, *Int. J. Adv. Manuf. Technol.*, 2012, **65**, p 1515–1528
 7. M. Guillo and M. Dubourg, Impact & Improvement of Tool Deviation in Friction Stir Welding: Weld Quality & Real-Time Compensation on an Industrial Robot, *Robot. Comput. Integr. Manuf.*, 2016, **39**, p 22–31
 8. X.J. Wang, D.B. Han, and Z.K. Zhang, Measurements and Influencing Factors of Longitudinal Force of Pin Tools in Friction Stir Welding Process, *Weld. Joining*, 2008, **9**, p 22–25
 9. X. Cao and M. Jahazi, Effect of Tool Rotational Speed and Probe Length on Lap Joint Quality of a Friction Stir Welded Magnesium Alloy, *Mater. Des.*, 2011, **32**, p 1–11
 10. D.Q. He, S.P. Li, J. Li, and S. He, Friction Stir Welding of 2024-T4 Aluminum Alloy Plate with 1.8 mm Thickness, *Hot Work. Technol.*, 2011, **40**, p 112
 11. H.H. Zhao, X.S. Feng, Y.Y. Xiong, G.Y. Su, L. Hu, and L.J. Guo, Microstructure and Properties of Micro Friction Stir Welded Joint of Al-Alloy Ultra Thin Plate with Zero Tilt Angle, *Trans. China Weld. Inst.*, 2014, **35**, p 47–51
 12. G.L. Qin, K. Zhang, W.B. Zhang, and C.S. Wu, Effect of Friction Stir Welding Heat Input on Weld Appearance and Mechanical Properties of 6013-T4 Al Alloy Joint, *Trans. China Weld. Inst.*, 2010, **31**, p 5–8
 13. D.Y. Yan, Q.Y. Shi, W.U. Aiping, J. Silvanus, Y. Liu, T. University et al., Numerical Analysis on the Residual Distortion of Al Alloy Sheet After Friction Stir Welding, *Acta Metall. Sin.*, 2009, **45**, p 183–188
 14. Z. Zhang, B.L. Xiao, and Z.Y. Ma, Influence of Water Cooling on Microstructure and Mechanical Properties of Friction Stir Welded 2014Al-T6 Joints, *Mater. Sci. Eng., A*, 2014, **614**, p 6–15
 15. D.Q. He and D.H. Li, Process Research and Microstructure Analysis on Friction-Stir Welding for LF21 Sheet, *Alum. Fabr.*, 2008, **2**, p 35–38
 16. S. Chen, H. Li, S. Lu, R. Ni, and J. Dong, Temperature Measurement and Control of Bobbin Tool Friction Stir Welding, *Int. J. Adv. Manuf. Technol.*, 2016, **86**, p 337–346
 17. Y.H. Zhao, J.D. Liu, L.N. Zhang, Z.S. Sun, and G.Q. Wang, Study on Friction Plug Welding of 2014 Aluminum Alloy FSW Joint, *J. Aeronaut. Mater.*, 2010, **30**, p 41–46
 18. Y.H. Zhao, S.B. Lin, L. Wu, and F.X. Qu, The Influence of Pin Geometry on Bonding and Mechanical Properties in Friction Stir Weld 2014 Al Alloy, *Mater. Lett.*, 2005, **59**, p 2948–2952
 19. I. Galvão, R.M. Leal, D.M. Rodrigues, and A. Loureiro, Influence of Tool Shoulder Geometry on Properties of Friction Stir Welds in Thin Copper Sheets, *J. Mater. Process. Technol.*, 2013, **213**, p 129–135
 20. Z. Zhang and H.J. Liu, Effect of Pin Shapes on Material Deformation and Temperature Field in Friction Stir Welding, *Hanjie Xuebao Trans. China Weld. Inst.*, 2011, **32**, p 5–8
 21. M.I. Costa, D. Verdera, J.D. Costa, C. Leitao, and D.M. Rodrigues, Influence of Pin Geometry and Process Parameters on Friction Stir Lap Welding of AA5754-H22 Thin Sheets, *J. Mater. Process. Technol.*, 2015, **225**, p 385–392
 22. M. Pakdil, G. Çam, M. Koçak, and S. Erim, Microstructural and Mechanical Characterization of Laser Beam Welded AA6056 Al-Alloy, *Mater. Sci. Eng. A*, 2011, **528**, p 7350–7356
 23. G. Çam, V. Ventzke, J.F.D. Santos, M. Koçak, G. Jennequin, P. Gonthier-Maurin, M. Penasa, and C. Rivezla, Characterization of Laser and Electron Beam Welded Al-Alloys, *Prakt. Metallogr.*, 2000, **37**, p 59–89
 24. G. Çam, V. Ventzke, J.F.D. Santos, M. Koçak, G. Jennequin, and P. Gonthier-Maurin, Characterisation of Electron Beam Welded Aluminium Alloys, *Sci. Technol. Weld. Joining*, 1999, **4**(5), p 317–323
 25. F.C. Liu and Z.Y. Ma, Influence of Tool Dimension and Welding Parameters on Microstructure and Mechanical Properties of Friction-Stir-Welded 6061-T651 aluminum alloy, *Metall. Mater. Trans. A*, 2008, **39**, p 2378–2388
 26. J.C. Song, L.Y. Ye, X.M. Zhang, D.Q. He, and H.P. Li, Influence of Cooling Conditions on Joint Properties of 2519A Aluminum Alloy by Friction Stir Welding, *J. Cent. South Univ.*, 2012, **43**(10), p 3801–3806